RESEARCH ARTICLE

WILEY

# Relations between structural and EEG-based graph metrics in healthy controls and schizophrenia patients

Javier Gomez-Pilar[1] | Rodrigo de Luis-García[2] | Alba Lubeiro[3] | Henar de la Red[4] | Jesús Poza[1,4,5,6] | Pablo Núñez[1] | Roberto Hornero[1,5,6] | Vicente Molina[3,4,5] (iD)

[1]Biomedical Engineering Group, University of Valladolid, Paseo de Belén, 15, 47011 Valladolid, Spain

[2]Imaging Processing Laboratory, University of Valladolid, Paseo de Belén, 15, 47011 Valladolid, Spain

[3]Psychiatry Department, School of Medicine, University of Valladolid, Av. Ramón y Cajal, 7, Valladolid 47005, Spain

[4]Psychiatry Service, Clinical Hospital of Valladolid, Ramón y Cajal, 3, Valladolid 47003, Spain

[5]Neurosciences Institute of Castilla y León (INCYL), Pintor Fernando Gallego, 1, 37007 University of Salamanca, 37007 Salamanca, Spain

[6]IMUVA, Mathematics Research Institute, University of Valladolid, Valladolid, Spain

**Correspondence**
Vicente Molina, Psychiatry Department, School of Medicine, University of Valladolid, Av. Ramón y Cajal, 7, 47005 Valladolid, Spain.
Email: vicente.molina@uva.es

## Abstract

Our aim was to assess structural and functional networks in schizophrenia patients; and the possible prediction of the latter based on the former. The possible dependence of functional network properties on structural alterations has not been analyzed in schizophrenia. We applied averaged path-length (PL), clustering coefficient, and density (D) measurements to data from diffusion magnetic resonance and electroencephalography in 39 schizophrenia patients and 79 controls. Functional data were collected for the global and theta frequency bands during an odd-ball task, prior to stimulus delivery and at the corresponding processing window. Connectivity matrices were constructed from tractography and registered cortical segmentations (structural) and phase-locking values (functional). Both groups showed a significant electroencephalographic task-related modulation (change between prestimulus and response windows) in the global and theta bands. Patients showed larger structural PL and prestimulus density in the global and theta bands, and lower PL task-related modulation in the theta band. Structural network values predicted prestimulus global band values in controls and global band task-related modulation in patients. Abnormal functional values found in patients (prestimulus density in the global and theta bands and task-related modulation in the theta band) were not predicted by structural data in this group. Structural and functional network abnormalities respectively predicted cognitive performance and positive symptoms in patients. Taken together, the alterations in the structural and functional theta networks in the patients and the lack of significant relations between these alterations, suggest that these types of network abnormalities exist in different groups of schizophrenia patients.

### KEYWORDS

brain network, diffusion magnetic resonance, dysconnectivity, electroencefalography, graph-theory, schizophrenia

## 1 | INTRODUCTION

Mental functions depend on global dynamics of cerebral networks (Dehaene & Changeux, 2011; Varela, Lachaux, Rodriguez, & Martinerie, 2001), whose functional and structural characteristics can be assessed in vivo using methods derived from graph-theory (Bullmore & Sporns, 2009). In this context, underpinnings of syndromes like schizophrenia likely involve distributed networks rather than regional alterations, as supported by studies using functional magnetic resonance imaging (fMRI) that revealed network alterations in the resting state (Lo et al.,

2015; Yu et al., 2011) and during task performance (Ma, Calhoun, Eichele, Du, & Adalı, 2012; Shim, Kim, Lee, & Im, 2014) in this syndrome. However, considering the rapid and transient change of functional integration of diverse cerebral regions in cognition in humans (Varela et al., 2001) and animals (Bressler, Coppola, & Nakamura, 1993), assessing fast change of cerebral networks in schizophrenia holds a great interest. Techniques with high temporal resolution are useful to this purpose: change of network properties using electroencephalographic (EEG) during a cognitive task was significantly decreased in schizophrenia patients (Gomez-Pilar et al., 2017). Using relative power analyses, we also reported lower EEG task-related change in theta but not in faster bands during an odd-ball task in schizophrenia (Bachiller et al., 2014).

As mentioned, methods derived from graph-theory are useful to assess the properties of cerebral networks, which can be summarized in parameters such as clustering coefficient (CLC) and characteristic path length (PL). In a binary network, local CLC is the ratio between the number of triangles in which a given node participates and the maximum possible number of triangles including that node. When CLC is averaged across the nodes of a network, it quantifies network segregation and local efficiency of information transfer. In turn, PL is the average of shortest distances for all possible pairs of nodes; it is likely related to information integration across areas. These network parameters provide complementary information about the properties of the whole brain network. Therefore, the use of these parameters instead of their corresponding nodal versions, allows to characterize the global and predominant changes of the network. A recent meta-analysis of functional graph-analytical studies in schizophrenia revealed significant decreases in measures of local organization (CLC) with preservation in short communication paths (PL) (Kambeitz et al., 2016).

Abnormalities in structural connectivity are also prevalent in schizophrenia (Ellison-Wright & Bullmore, 2009). These abnormalities are likely reflected in structural network properties, since longer structural PL values were found in schizophrenia at frontal and temporal regions using dMRI (van den Heuvel, Mandl, Stam, Kahn, & Hulshoff Pol, 2010) and may be associated to genetic liability to this disorder (Bohlken et al., 2016). Thus, the possibility exists that functional network alterations might be secondary to structural abnormalities in schizophrenia. Indeed, in this syndrome, a relationship has been reported between a reduction in "rich-club density" (i.e., connections among high-degree hub nodes) and global efficiency of functional connectivity in the resting state using fMRI (van den Heuvel et al., 2013). Similarly, connectivity deficits in rich-club hubs have been described in young offspring of schizophrenia patients associated to disruption of the functional connectome (Collin, Scholtens, Kahn, Hillegers, & van den Heuvel, 2017). However, functional connectivity alterations in schizophrenia are not necessarily determined by structural connectivity, since functional connections in the resting state can be found between regions without direct anatomical connections (Honey et al., 2009).

The application of graph-theory parameters to functional and structural measurements can yield complementary information and help uncovering hidden relationships (Sui, Yu, He, Pearlson, & Calhoun, 2012). Using diffusion MRI (dMRI), graph-theory parameters may inform about structural connectivity differences between anatomical structures, revealing highly connected hubs (Honey, Thivierge, & Sporns, 2010). Graph-theory parameters applied to functional analysis may reveal baseline network characteristics and its dynamic modulation during cognition of signals such as synchrony of the bold-oxygen level dependent signal between regions, or magneto-electrical signals between sensors. Considering the millisecond-scale of modulation of cortical activity during cognition (Bressler et al., 1993; Dehaene & Changeux, 2011), the combination of network analyses with temporal resolution of EEG recordings can be useful to assess this task-related modulation. Indeed, using EEG in healthy subjects, we reported a significant task-related modulation of network parameters from prestimulus (from −300 to 0 ms prior to stimulus onset) to response (from 150 to 450 ms poststimulus) windows (Martin-Santiago et al., 2016) during an odd-ball task.

To our knowledge, no previous study has assessed the relationship between structural and EEG networks in schizophrenia. Such investigation may help identifying the substrate of the cortical dysfunction in schizophrenia. Therefore, this study was aimed at characterizing the properties of structural and EEG-based functional networks in schizophrenia and assessing the relationships between properties of those networks in this syndrome, particularly between structural connectivity and EEG modulation.

## 2 | SUBJECTS AND METHODS

### 2.1 | Subjects

A total of 39 schizophrenia (19 stable chronic and 20 first-episode, FE) patients and 78 healthy controls with normal hearing were included. Demographic, clinical, cognitive and EEG data were collected for each participant (Table 1). In addition, dMRI data were also available in 33 patients (16 FE) and 27 controls (Table 1). One of the psychiatrists in the group (VM) diagnosed the patients according to the Diagnostic and Statistical Manual of Mental Disorders, 5th edition. Chronic patients received atypical antipsychotics, 30 of them in monotherapy (12 received antidepressants and 7 benzodiazepines). FE patients were receiving stable doses of antipsychotics for <15 days, with a wash-out period of 24 hr prior to EEG acquisition. This was so done to minimize the possible effects of treatment in this group, given their relatively short exposure to antipsychotics. Symptoms were scored using the Positive and Negative Syndrome Scale (PANSS) (Kay, Fiszbein, & Opler, 1987). Exclusion criteria were: (a) any neurological illness; (b) history of cranial trauma with loss of consciousness longer than 1 min; (c) past or present substance abuse, except nicotine or caffeine; (d) total intelligence quotient (IQ) smaller than 70; (e) for patients, any other psychiatric process; and (f) for controls, any current psychiatric or neurological diagnosis or treatment.

The population here included overlaps in part with that of previous reports of our group in schizophrenia on functional networks based on evoked response (Gomez-Pilar et al., 2017), graph complexity (Gomez-Pilar et al., 2018) and structural connectivity of specific tracts of the prefrontal region (Molina et al., 2017)

**TABLE 1** Demographic, clinical and cognitive data in patients and controls

| | Schizophrenia | | Controls | |
|---|---|---|---|---|
| | Schizophrenia (EEG, n = 39) | Schizophrenia (EEG + dMR; n = 33) | Controls (EEG; n = 78) | Controls (dMR + EEG; n = 27) |
| Age | 33.053 (8.801) | 33.059 (8.951) | 30.948 (10.839) | 34.668 (11.150) |
| Sex (M:F) | 23:16 | 19:14 | 46:32 | 18:9 |
| CPZ equivalents (mg/d) | 377.901 (196.934) | 374.802 (193.419) | NA | |
| Duration(months) | 95.169 (117.388) | 83.86 (117.456) | NA | |
| Education years | 14.191 (3.600) | 14.882 (3.051) | 16.561 (2.254) | 17.427 (2.866) |
| PANSS positive symptoms | 11.702 (3.427) | 11.388 (3.457) | NA | |
| PANSS negative symptoms | 17.571 (7.309) | 15.450 (5.057) | NA | |
| Total symptoms | 53.810 (18.892) | 53.313 (18.913) | NA | |
| Total IQ | 91.061 (14.528)*** | 94.701 (11.789)*** | 113.209 (11.088) | 109.458 (12.165) |
| Verbal memory | 34.262 (12.889)*** | 35.315 (12.345)*** | 51.115 (8.194) | 53.000 (7.274) |
| Working memory | 16.151 (5.010)*** | 17.074 (4.148)*** | 21.626 (3.621) | 23.140 (2.723) |
| Motor speed | 58.879 (13.781)*** | 62.538 (12.041)*** | 72.610 (16.583) | 85.503 (8.154) |
| Verbal fluency | 18.352 (5.730)*** | 19.613 (4.799)*** | 27.856 (5.155) | 28.827 (5.177) |
| Processing speed | 43.700(15.360)*** | 45.641 (14.672)*** | 69.588 (14.378) | 69.251 (14.841) |
| Problem solving | 15.253 (4.622) | 16.317 (3.418) | 17.524 (2.571) | 17.042 (2.641) |
| WCST perseverative errors (%) | 17.921 (10.123)*** | 21.152 (17.077)*** | 9.801 (5.141) | 8.221 (3.573) |
| WCST completed categories | 4.419 (1.878)*** | 4.812 (1.711)** | 5.847 (0.610) | 5.879 (0.478) |

Significant differences with respect to controls are shown for patients $*p < .05$; $**p < .001$; $***p < .001$

We obtained written informed consent from all participants after full printed information. The ethical committee of the University Hospital of Valladolid approved the study.

## 2.2 | Cognitive assessment

Cognitive data from patients and controls were collected using: the Wechsler Adult Intelligence Scale, WAIS-III (IQ); the Wisconsin Card Sorting Test (WCST; completed categories and percentage of perseverative errors); and the Spanish version of the Brief Assessment in Cognition in Schizophrenia Scale (BACS) (Segarra et al., 2011).

## 2.3 | MRI acquisition and processing

Acquisitions were carried out using a Philips Achieva 3 Tesla MRI unit (Philips Healthcare, Best, The Netherlands) at the MRI facility at Valladolid University, including anatomical T1-weighted and diffusion-weighted images. For the T1-weighted images, acquisition parameters were: turbo field echo sequence, $256 \times 256$ matrix size, $1 \times 1 \times 1$ mm$^3$ of spatial resolution and 160 slices covering the whole brain. About the diffusion-weighted images (DWIs), the acquisition protocol parameters were: 61 gradient directions and one baseline volume, b-value = 1,000 s/mm$^2$, $2 \times 2 \times 2$ mm$^3$ of voxel size, $128 \times 128$ matrix and 66 slices covering the entire brain. Total acquisition time was 18 min.

The processing pipeline of the acquired MRI volumes is designed to obtain structural connectivity matrices by using both the anatomical (T1-weighted) and diffusion images (Figure 1).

First, nonbrain structures were removed from the T1 images, using BET, the brain extraction tool from the FSL software suite (http://fsl.fmrib.ox.ac.uk) (Smith, 2002). After that, the segmentation of 84 cortical structures was performed employing Freesurfer (https://surfer.nmr.mgh.harvard.edu) (Desikan et al., 2006; Fischl et al., 2004). From the same T1 images, gray matter, white matter, and cerebrospinal fluid were also segmented, and subcortical gray matter structures were obtained using FMRIB's Automated Segmentation Tool (FAST) and FMRIB's Integrated Registration and Segmentation Tool (FIRST) utilities from FSL, respectively (Patenaude, Smith, Kennedy, & Jenkinson, 2011; Zhang, Brady, & Smith, 2001), and combined into a volume called 5tt (5-tissue-type) image.

In parallel, the brain was extracted from the DWIs using DWI2-MASK tool from MRtrix (www.mrtrix.org) (Dhollaner & Connelly, 2016). Also employing MRtrix, orientation distribution functions were estimated from the diffusion data using spherical deconvolution (Tournier, Calamante, & Connelly, 2007), which were later employed to generate anatomically constrained tractography using both the diffusion data and the 5tt image (after registration). Two million streamlines were generated for each subject.

In order to characterize diffusion at each voxel, diffusion tensors were estimated using a least squares method (Salvador et al., 2005),
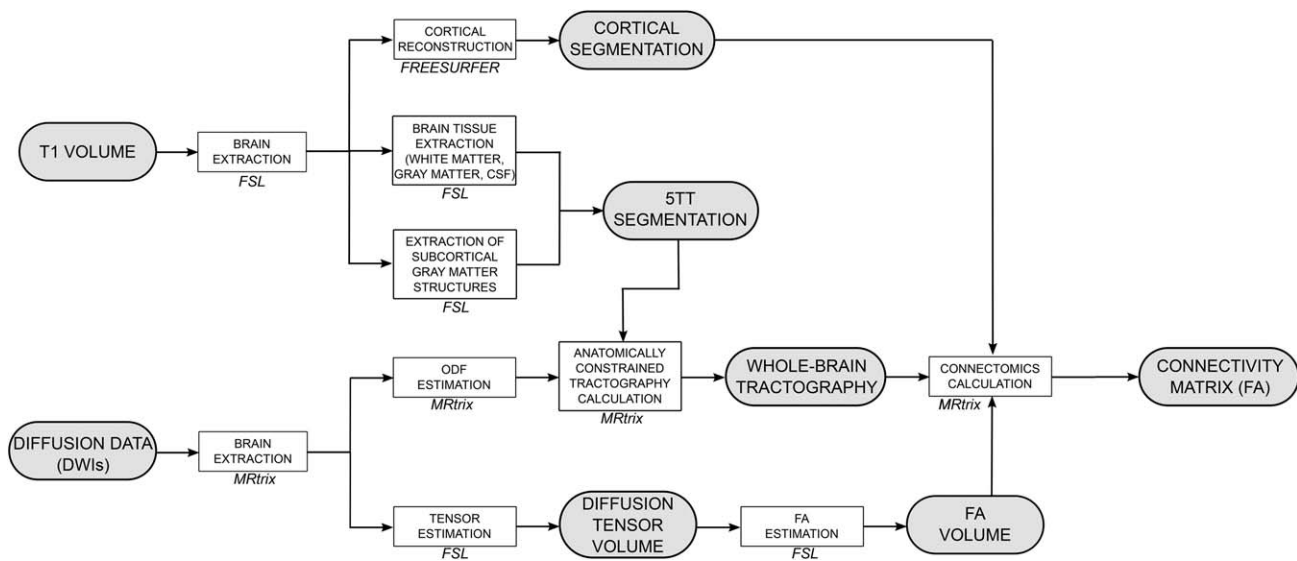
**FIGURE 1** Processing pipeline yielding FA values to be used in graph-theory calculations

and scalar fractional anisotropy (FA) volumes were computed from the diffusion tensors. FA quantifies the amount of anisotropy in the diffusion tensor, that is, how much it deviates from a totally isotropic diffusion. FA is usually interpreted as a descriptor of white matter integrity, and decreases in FA have been related to alterations in the white matter due to several factors (demyelination and axonal destruction, among others).

Finally, connectivity matrices were constructed from the tractography results and the (registered) cortical segmentations. When a streamline between two cortical segmentations was found, the averaged FA was computed. Thus, 84 × 84 connectivity matrices were obtained using FA as connectome metrics (Figure 2). A threshold was not applied to the obtained matrices; however, some matrix coefficients were equal to zero when a streamline was not found.

Similar connectomics analyses have been reported in schizophrenia (Di Biase et al., 2017) and other neurocognitive conditions (Jones et al., 2015)

## 2.4 | EEG recordings and processing

### 2.4.1 | EEG acquisition and preprocessing

EEG recordings were obtained following MRI scans, after a resting period of 30 min. Participants performed a 13 min three-tone P300 oddball task (for a detailed description see (Gomez-Pilar et al., 2017).
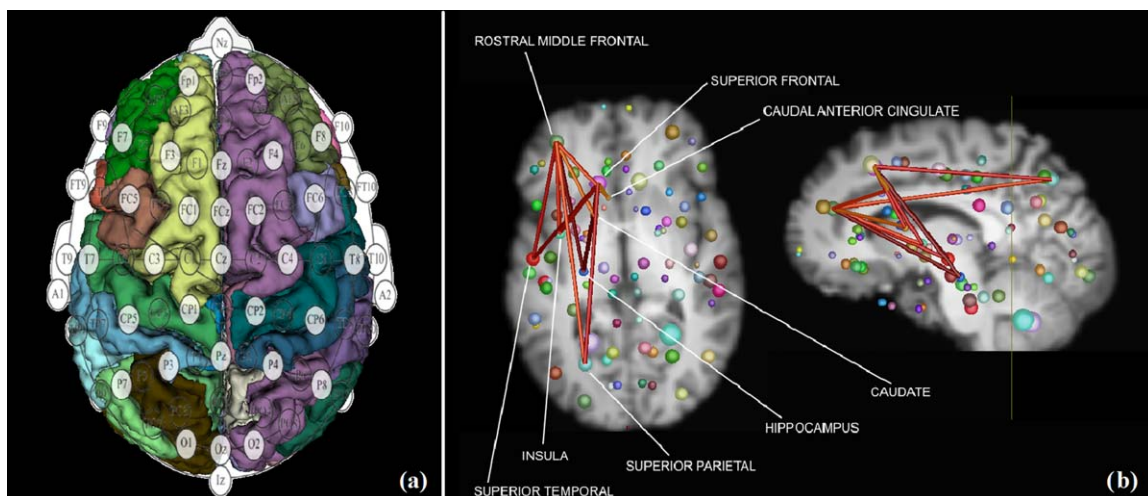


**FIGURE 2** (a) The 29 EEG channel labels superposed on the structural ROIs. EEG nodes (filled in white) were used to generate functional connectivity matrices from PLV values between each pair of electrodes. The figure illustrates the approximate placement of the EEG electrodes over the ROIs. The list of the 29 electrodes used in the study according to international 10-10 system is: Fp1, Fp2, F7, F3, Fz, F4, F8, FC5, FC1, FCz, FC2, FC6, T7, C3, Cz, C4, T8, CP5, CP1, CP2, CP6, P7, P3, Pz, P4, P8, O1, Oz and O2. (b) Schematic depiction (axial and sagittal views) of the relevant tracts (streamlines) from which FA was calculated to generate structural connectivity matrices. Streamlines were calculated between each pair of the 84 nodes corresponding to the cortical segmentation are shown as spheres (their sizes are proportional to the actual size of the corresponding ROI). For the sake of clarity, only tracts linking PFC with anterior cingulate, superior temporal, insular, and superior parietal cortices and hippocampus and caudate are drawn [Color figure can be viewed at wileyonlinelibrary.com]

Electrode impedance was always kept under 5 kΩ. Ground was placed at Fpz electrode and each channel was referenced over Cz electrode and re-referenced to the average activity of all active sensors (Bledowski et al., 2004; Gomez-Pilar et al., 2018), yielding a total of 29 channels.

The P300 task has several advantages for assessing functional network modulation in schizophrenia. In addition to its widespread previous use in the field: (a) it is easy to perform, thus decreasing bias related to lack of subject's cooperation; (b) its performance activates a large cerebral network (Bledowski et al., 2004; Linden et al., 1999); and (c) differences in EEG global activation patterns have been reported in schizophrenia using this paradigm (Gomez-Pilar et al., 2017).

Signals were band pass filtered between 1 and 70 Hz. In addition, a zero-phase 50 Hz notch filter was used to remove the power line artifact. A three-step artifact rejection algorithm was applied to minimize electroculographic and electromiographic contamination (Bachiller et al., 2015a): (a) an independent component analysis (ICA) was carried out to discard noisy ICA components; (b) after ICA reconstruction, EEG signals were divided into trials of 1 s length (ranging from 300 before to 700 ms after stimulus onset); and (c) an automatic method was applied to reject trials whose amplitude exceeded an adaptive statistical-based threshold, which consists of two stages. First, the mean and standard deviation of each channel was computed. Then, trials that exceeded mean $\pm 4 \times SD$ in at least two channels were discarded (Nunez et al., 2017). After this adaptive artifact rejection, $91.21 \pm 11.28$ trials for controls—with a median (interquartile range) of 91 (85 97) trials—and $86.33 \pm 14.13$ – with a median (interquartile range) of 86 (76.75 94)—were left for further analyses ($p = .051$, Mann-Whitney $U$-test).

In order to describe the event-related potential (ERP) waveforms, Supporting Information Figure S1 has been include in the Supplementary material. ERPs in the midline electrodes are shown in Supporting Information Figure S1A. Supporting Information Figure S1B shows the channel grand average waveforms. Finally, Supporting Information Figure S1C depicts scalps maps with the P300 peak amplitude for both groups.

### 2.4.2 | EEG brain graphs

The functional brain network was characterized using EEG graphs. Electrodes were used to represent network nodes, whereas network edges were set by computing the neural coupling between pairs of electrodes. Specifically, neural coupling was established using the phase-locking value (PLV) across successive trials (Lachaux, Rodriguez, Martinerie, & Varela, 1999). PLV in sensible to small oscillations of the EEG (Spencer et al., 2003) and takes into account nonlinearities (van Diessen et al., 2015), which is an intrinsic feature of EEG recordings. PLV can be computed using different approaches. In this study, the continuous wavelet transform (CWT) was used to extract the phase information from each trial (Bob, Palus, Susta, & Glaslova, 2008). Edge effects in CWT were considered by computing the cone of influence (COI) for prestimulus and response time windows. Only wavelet coefficients inside the respective COI were considered for the analyses to avoid edge effects. We refer to our previous studies (Gomez-Pilar

et al., 2018) for detailed explanations about how wavelet coefficient were computed, the wavelet parameters were configured and the COIs were applied to the CWT decomposition in order to minimize edge effects. After using CWT approach to perform filtering and phase extraction in one operation (Bob et al., 2008), the PLV between two signals $x(t)$ and $y(t)$ can be obtained evaluating the variability of the phase difference across successive trials:

$$\text{PLV}_{xy}(k,s) = \frac{1}{Nt} \left| \sum_{n=1}^{N} e^{\Delta\varphi_{xy}(k,s,n)} \right|, \tag{1}$$

where $N_t$ is the number of trials, $\Delta\varphi_{xy}$ is the instantaneous phase difference between $x$ and $y$ signals, $k$ is the time interval, and $s$ the scaling factor of the mother wavelet (see Bachiller et al., 2015a,b for details).

Thus, functional connectivity matrices based on PLV ranged between 0 and 1, where a value of 1 is obtained with completely synchronized signals and a value of 0 implies an absence of synchronization. Following the same methodology as in the structural data, functional connectivity matrices were not thresholded.

### 2.4.3 | Segmentation of the EEG response

In order to assess the task-related modulation of the graph parameters along the odd-ball task, two-time windows were considered for comparison. On the one hand, the prestimulus window (i.e., a period of expectation before the stimulus onset) ranges from −300 ms to the stimulus onset. On the other hand, the response window was selected to capture the P3b response. In order to take into account, the inter-individual variability of the P3b response, the response window was adaptively set for each participant. First, the event-related wave was computed for each subject by the synchronized averaging of all the trials corresponding to attended target tones. Second, a low-pass finite impulse response filter with cut-off frequency of 8 Hz was applied to the evoked wave in order to obtain only the components related to delta and theta frequency bands. It is noteworthy that this filter was only applied to estimate the time window related to the EEG response. Thirdly, the maximum amplitude of the low-pass filtered evoked wave in the Pz channel was located into a window ranging from 250 to 550 ms from the stimulus onset (Bachiller et al., 2015b). The corresponding sample to the maximum amplitude was used as a central time sample of the response window. Finally, the response window was set on $\pm 150$ ms around the central time sample.

## 2.5 | Graph-theory parameters

From both the structural and functional connectivity matrices, we calculated three graph-theory parameters to characterize global properties of the brain network: (a) connectivity strength (i.e., mean network degree) by means of network density (D), also named network strength (b) network segregation using CLC, and (c) network integration by means of PL (Rubinov & Sporns, 2010). For the sake of comparability and to obtain results independent of network size and network strength, CLC and PL were computed over an ensemble of 50

surrogate random networks, which were used to normalize CLC and PL values obtained from the original networks (Stam et al., 2009).

Therefore, normalized CLC and PL can be defined:

$$CLC = \frac{C}{C^{random}}, \tag{2}$$

$$PL = \frac{L}{L^{random}}, \tag{3}$$

where $C$ and $L$ can be defined as follows:

$$C = \frac{1}{N} \sum_{i=1}^{N} \frac{\sum_{i \neq j} \sum_{\substack{i \neq l \\ j \neq l}} w_{ij} w_{il} w_{jl}}{\sum_{i \neq j} \sum_{\substack{i \neq l \\ j \neq l}} w_{ij} w_{il}}, \tag{4}$$

$$L = \frac{N(N-1)}{\sum_{i=1}^{N} \sum_{j \neq i}^{N} \frac{1}{L_{ij}}}, \tag{5}$$

In Equation 4, $w_{ij}$ can be referred to PLV between nodes $i$ and $j$ (for functional analyses) or the structural connectivity between two regions using the streamlines from MRI. $N$ is the total number of nodes of the network (29 in EEG analyses, 84 in MRI). Finally, $L_{ij}$ is defined as the inverse of the edge weight (Stam et al., 2009).

With regard to the EEG functional network, parameters were computed into two frequency ranges. They were selected based on their relevance for the task-related modulation of the EEG during P300 tasks shown in schizophrenia in previous studies: the global band (from 1 to 70 Hz) (Gomez-Pilar et al., 2017) and the theta band (from 4 to 8 Hz) (Bachiller et al., 2014; Doege et al., 2009). A diminished task-related modulation of theta activity during an oddball task was found in schizophrenia, but not in faster frequency bands (Bachiller et al., 2014). In addition, the assessment of the theta band showed abnormalities in the brain network reconfiguration in the secondary functional pathways in schizophrenia (Gomez-Pilar et al., 2018). On the other hand, the global band could be also useful to assess the specificity of the theta band.

Functional network parameters during prestimulus and its corresponding task-related modulation (i.e., difference between the response and the prestimulus windows) were used for statistics.

Structural connectivity network parameters will be referred to as dMRI-PL, dMRI-D, and dMRI-CC, and functional network parameters as EEG-PL, EEG-D, and EEG-CLC.

## 2.6 | Statistics

We compared socio-demographic data (age, sex, education years, and parental education) between patients and controls ($t$ or $\chi^2$ tests when appropriate). Each subgroup of patients (i.e., those with only EEG and those with EEG plus dMRI data) was compared with the corresponding controls.

### 2.6.1 | Comparisons of graph-theory parameters

After testing normality and homoscedasticity of data distribution using Kolmogorov-Smirnov and Levene tests, we compared functional (EEG-based) and structural (dMRI-based) graph-theory parameters between patients and controls using Student's $t$-tests. Within-group changes in functional network parameters were assessed using $t$-tests for related samples. After Bonferroni adjustment, $p$ level was set to $.05/15 = .003$.

For the sake of interpretability, we studied the relationship between structural connectivity parameters (dMRI-PL, dMRI-D, and dMRI-CLC) and the average FA values in identifiable relevant white matter tracts. With this analysis, it could be easier to interpret the results of graph-theory data in terms of integrity of white matter tracts. To do this, we used the methodology employed in a previous study (Molina et al., 2017), in which FA was assessed in tracts connecting prefrontal cortex (PFC) with other relevant regions. Correlation coefficients between structural connectivity network parameters and FA values in these tracts were computed, with Bonferroni adjustment with $p$ set to .001.

When statistically significant differences in network parameters were found between patients and controls, we compared the corresponding values between FE and stable chronic patients using Mann-Whitney U-tests for independent samples, to discard a major effect of chronicity in those differences.

### 2.6.2 | Association between structural and functional networks

The main hypothesis of the study was that the structural connectivity of the brain network would determine the prestimulus functional network properties and/or its task-related modulation. This was studied using stepwise multivariate regression models. Since significant correlations between different structural variables were found, to avoid collinearity effects we performed principal component analyses (PCAs) separately with structural (dMRI) and functional (EEG) variables for global and theta bands. This allowed a priori reducing the number of comparisons for further analyses, thus reducing the Type I errors risk. Individual structural and functional network factor scores were introduced respectively as independent and dependent variables in the regression model aimed to predict functional properties from structural network data.

### 2.6.3 | Clinical and cognitive correlates

Next, we studied the cognitive and clinical correlates of graph-theory parameters for the patients using stepwise multivariate regression models (for structural and functional data). To calculate a global score summarizing cognition, individual cognitive scores were introduced in a PCA. The resulting individual scores were saved and introduced as dependent variables in the model. Possible associations between graph-theory parameters and symptoms were similarly assessed.

To discard major confounders, correlation coefficients were calculated between graph-theory parameters and both illness duration and current treatment doses.

## 3 | RESULTS

There were no statistically significant differences between patients and controls in age and sex distribution in the whole sample, nor between
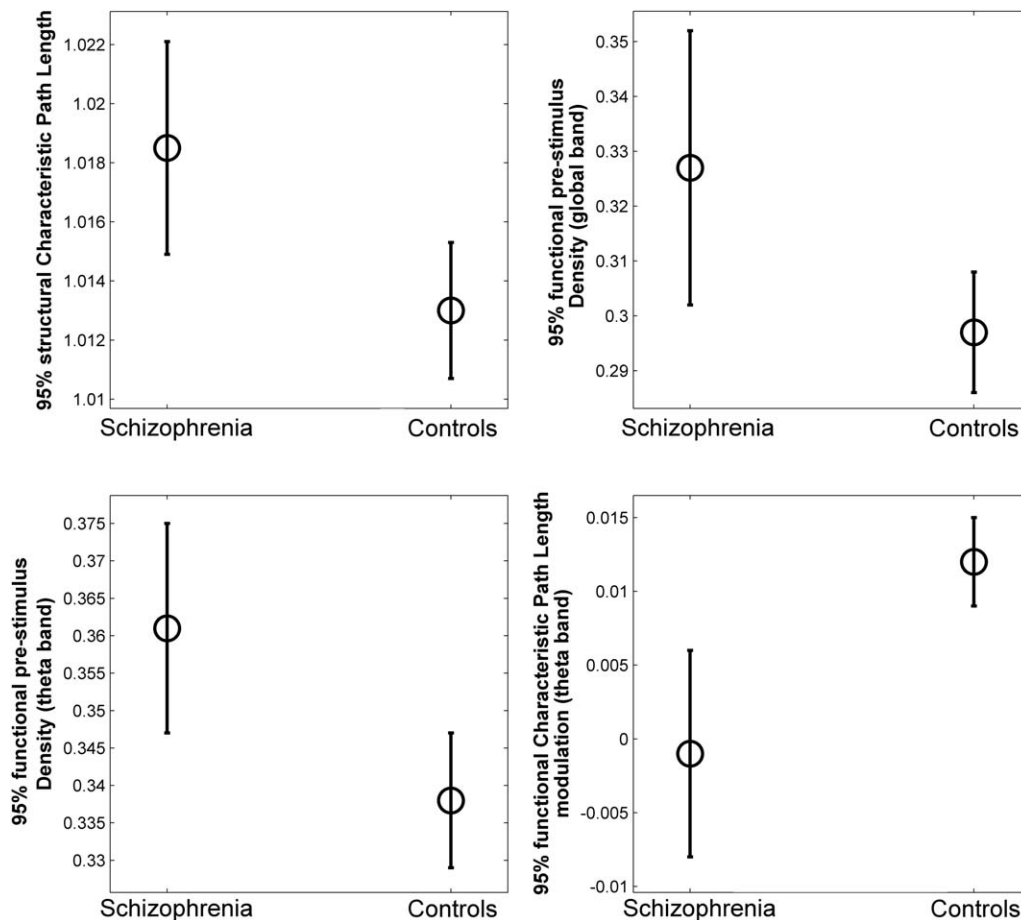
**FIGURE 3** Error bars corresponding to the graph-theory parameters with statistically significant differences between patients and controls (from left to right, structural PL, functional prestimulus D at the global and at the theta bands, and functional PL task-related modulation at the theta band). Circles represent the mean value, while bars indicate the interval of confidence (95%)

patients and controls with dMRI data. Patients had fewer study years and a generalized cognitive deficit (Table 1).

## 3.1 | Comparison of graph-theory parameters

### 3.1.1 | Structural parameters

Patients showed statistically significant longer mean dMRI-PL values than controls ($t = 2.20$, $df = 58$, unadjusted $p = .03$; Figure 3).

Values of dMRI-PL were inversely associated to FA values in relevant tracts linking PFC with anterior cingulate, superior temporal, insular and superior parietal cortices and hippocampus and caudate. Moreover, dMRI-CLC and dMRI-D values were directly associated to FA values in these tracts (see Section 3.2.3).

### 3.1.2 | Functional parameters

Both EEG-PL and EEG-CLC in the global band and EEG-D in the theta band showed a significant increase from prestimulus to response within patients and control groups, which remained significant only in the controls after Bonferroni adjustment (Table 2). Controls, but not patients, showed a significant increase in EEG-CLC and EEG-PL values in the theta band from prestimulus to response (Table 2). Therefore, a

significant positive task-related modulation of EEG-CLC and EEG-PL values was found in this band only in controls.

In the global band, prestimulus window EEG-D was significantly higher for patients ($t = 2.52$, $df = 115$, unadjusted $p = .03$; Figure 3; Table 2), without significant differences in the corresponding task-related modulation.

In the theta band, prestimulus EEG-D was higher ($t = 2.637$, $df = 115$, $p = .010$), and EEG-PL task-related modulation was lower ($t = -2.128$, $df = 115$, $p = .035$) for patients (Figure 3; Table 2)

Between-group differences in functional and structural graph-theory parameters had medium effect sizes (Cohen's $d$; Table 2), although these differences would not survive after Bonferroni adjustment.

### 3.1.3 | Comparison between FE and chronic patients

As compared with the FE subgroup, we found larger structural PL in the chronic patients, while no differences were obtained between patient subgroups in global and theta band prestimulus density nor in theta band modulation (Supporting Information Table S3).

**TABLE 2** Structural and functional graph-theory parameters for patient and controls

| | | Structural (dMRI) network | | | Functional (EEG) network | | | | | | |
| | | Schizophrenia (n = 33) | Controls (n = 27) | Cohen's d | Global band | | | Theta band | | |
| | | | | | Schizophrenia (n = 39) | Controls (n = 78) | Cohen's d | Schizophrenia (n = 39) | Controls (n = 78) | Cohen's d |
|---|---|---|---|---|---|---|---|---|---|---|
| CLC | | 0.995 (0.002)** | 0.995 (0.001) | | | | | | | |
| | Prestimulus | | | | 1.006 (0.004) | 1.007 (0.005) | | 1.009 (0.006) | 1.008(0.004) | |
| | Modulation | | | | 0.001 (0.001)* | 0.001 (0.002)*** | | −8.526E-05 (0.004) | 0.001 (0.004)* | |
| PL | | 1.018(0.009)** | 1.013 (0.005) | 0.686 | | | | | | |
| | Prestimulus | | | | 1.087 (0.028) | 1.088 (0.027) | | 1.104(0.027) | 1.099 (0.022) | |
| | Modulation | | | | 0.003 (0.008)* | 0.004 (0.013)*** | | −0.001 (0.020)** | 0.009 (0.025)* | −0.432 |
| D | | 0.329 (0.032) | 0.346 (0.030) | | | | | | | |
| | Prestimulus | | | | 0.326 (0.078)* | 0.297 (0.053) | 0.434 | 0.361 (0.043)** | 0.3381 (0.042) | 0.514 |
| | Modulation | | | | 0.001 (0.009) | −0.001 (0.013) | | 0.008 (0.025)* | 0.020 (0.032)* | |

Mean values are shown with the corresponding SD per group. Task-related modulation is defined as the difference for the corresponding functional parameter between its value at the response and prestimulus windows.

a**Statistically significant within-group task-related modulation (response minus prestimulus; p < .05; **Statistically significant differences between patients and controls (p < .05); *** idem p < .001.

## 3.2 | Association between structural and functional networks

### 3.2.1 | Correlations among graph-theory parameters: PCA

Correlations were high among graph-theory parameters based on structural (dMRI-CLC vs. dMRI-D $r = .802$, $p < .001$; dMRI-CLC vs. dMRI-PL $r = −.515$, $p < .001$) and functional data in the global (EEG-CLC vs. EEG-PL $r = .791$, EEG-CLC vs. EEG-D $r = .512$, $p < .001$) and in the theta bands (EEG-CLC vs. EEG-PL $r = .919$, $p < .001$; EEG-CLC vs. EEG-D $r = .631$, $p < .001$). Therefore, independent variables for the regression models were calculated from PCAs. Eigenvalues higher than the unit and scree-plots were used to select the number of factors, saving individual factor scores. PCA results are summarized in Supporting Information Table S2.

The PCA for structural parameters yielded one factor explaining 73.07% of variance (eigenvalue 2.192), with positive coefficients for dMRI-CLC and dMRI-D and negative for dMRI-PL. Factor scores were statistically significant lower for patients (mean −0.235, SD 1.125) than for controls (mean 0.294, SD 0.769; $df = 54$, $t = 2.01$, $p = .049$).

PCA of EEG graph-theory parameters in the global band yielded a three factors solution explaining 88.49% of variance, respectively contributed by EEG-CLC, EEG-PL, and EEG-D task-related modulation (42.40% variance, eigenvalue 2.544), prestimulus EEG-PL and EEG-CLC (25.39% variance, eigenvalue 1.52) and both prestimulus and task-related modulation of EEG-D (20.70% variance, eigenvalue 1.242). Scores for the third factor were significantly larger for patients (mean 0.300, SD 1.138) than for controls (mean −0.134, SD 0.893, $t = 2.26$, $df = 115$, $p = .026$).

In the theta band, a two-factor solution was found. The first was positively related to task-related modulation of EEG-CLC, EEG-PL and EEG-D (53.07% variance, eigenvalue 3.18), whereas the second factor was positively related to prestimulus EEG-CLC, EEG-PL, and EEG-D (23.55% variance, eigenvalue 1.41). Scores for the first factor were smaller at trend level for patients (mean −0.294, SD 0.759) than for controls (mean 0.119, SD 1.090, $t = −1.86$, $df = 115$, $p = .065$).

### 3.2.2 | Prediction of functional scores based on structural scores

For the healthy controls, structural factor scores predicted functional global band prestimulus (EEG-PL and EEG-CLC) scores ($R^2 = 0.222$, $df = 1,24$, $F = 6.86$, $β = −0.472$, $p = .015$). This relation was not significant for patients ($R^2 = .008$, $df = 1,29$, $F = 0.23$, $β = −0.090$, $p = .606$).

In the patients, structural factor scores inversely predicted values of the first factor in the global band (task-related modulation of EEG-PL and EEG-CLC) ($R^2 = .172$, $df = 1,29$, $F = 6.03$, $β = −0.415$, $p = .02$; Figure 4a). Therefore, in the patients, larger dMRI-CLC and dMRI-D values were associated to smaller task-related modulation of EEG-PL and EEG-CLC. Since dMRI-PL contributed negatively to the structural factor, that negative association between structural and functional factors implies that shorter dMRI-PL will predict larger EEG-PL and EEG-CLC task-related modulation.

In the patients structural factor scores did not predict functional parameters that had shown significant differences with controls: task-
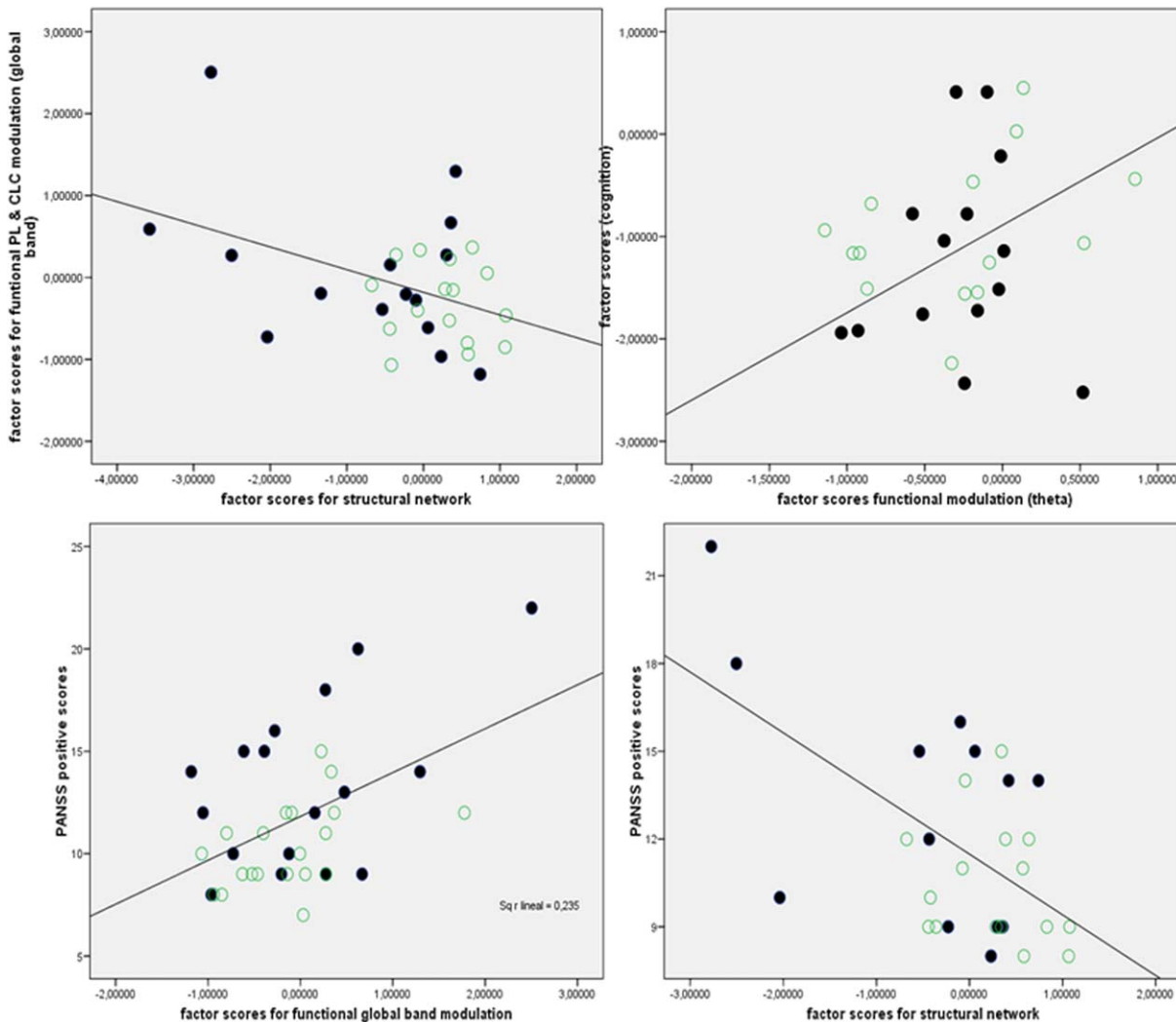
**FIGURE 4** Scatterplots showing the association between (a) factor scores resulting from the PCA of structural graph-theory parameters (X axis) and scores of the second factor resulting from the PCA of functional graph-theory parameters in the global band (modulation; Y axis); (b) factor scores for the first factor from the PCA of functional graph-theory parameters at the theta band (modulation) and factor scores from the PCA summarizing cognitive scores; (c) positive PANSS scores and global band PL and CLC task-related modulation and (d) structural network (right) Solid dots represent chronic patients, open dots represent FE patients [Color figure can be viewed at wileyonlinelibrary.com]

related modulation in the theta band ($R^2 = 0.001$, $df = 1,29$, $F = 0.006$, $β = 0.015$, $p = .93$), prestimulus EEG-D in the global band ($R^2 = 0.024$, $df = 1,29$, $F = .075$, $β = −0.15$, $p = .42$) and prestimulus (EEG-CLC, EEG-PL, and EEG-D) in the theta band ($R^2 = 0.008$, $df = 1,29$, $F = 0.244$, $β = 0.091$, $p = .34$).

For the sake of interpretability, we calculated Pearson's correlations between individual d-MRI and EEG graph parameters. dMRI-CLC was negatively associated in the patients to task-related modulation of EEG-PL ($r = −.383$, $p = .03$) and EEG-PL ($r = −.495$, $p = .005$) in the global band. There were no significant correlations between task-related modulation in theta band parameters and individual dMRI-based graph parameters ($−.28 > r > .166$).

### 3.2.3 | Structural networks and specific tracts

Structural PL was inversely associated to FA ($n = 55$) in the tracts linking homolaterally dorsolateral PFC with right cingulate ($r = −.299$, $p = .028$), left cingulate ($r = −.357$, $p = .008$), right hippocampus ($r = −.499$, $p < .001$), left caudate ($r = −.446$, $p = .001$), left parietal ($r = −.394$, $p = .003$), left superior temporal ($r = −.359$, $p = .007$), right superior temporal ($r=-0.478$, $p < 0.001$), left insula ($r = −.322$, $p = .016$) and right insula ($r = −.359$, $p = .007$). No positive correlations were found between structural PL and FA values.

Structural CLC was directly related to FA in the tracts linking homolaterally dorsolateral PFC with right hippocampus ($r = .508$, $p < .001$), left parietal ($r = .392$, $p = .003$) and right parietal ($r = .273$, $p = .044$). Similarly, structural density was directly related to FA in the tracts linking homolaterally dorsolateral PFC with left hippocampus ($r = .328$, $p = .016$), right hippocampus ($r = .404$, $p = .002$), left thalamus ($r = .337$, $p = .013$), left caudate ($r = .268$, $p = .050$), left parietal ($r = .542$, $p < .001$), right parietal ($r = .435$, $p = .001$), left superior temporal ($r = .331$, $p = .014$), right superior temporal ($r = .475$, $p < .001$), left insula ($r = 0.316$, $p = 0.019$) and right insula ($r = .424$, $p = .001$).

Only associations at $p \leq .001$ were significant after Bonferroni adjustment.

## 3.3 | Cognitive and clinical correlates

The factor analysis of cognitive scores yielded a single factor (eigenvalue 3.449), with positive coefficients for all but percent of perseverative errors, explaining 54.11% of the total variance.

Scores of the first factor in the theta band (modulation) directly predicted cognitive performance in the patients ($R^2 = 0.312$, $df = 1,28$, $\beta = 0.558$, $F = 12.22$, $p = .002$; Figure 4b). Structural values were not associated to cognition in patients.

Positive symptoms were inversely associated to structural network factor scores ($R^2 = 0.329$, $df = 1,29$, $F = 13.21$, $\beta = -0.573$, $p = .001$; Figure 4c), therefore positively associated to dMRI-CLC and dMRI-D and inversely to dMRI-PL. The first factor in the global band (task-related modulation of EEG-PL and EEG-CLC) positively predicted positive symptoms ($R^2 = 0.235$, $df = 1,35$, $F = 10.74$, $\beta = -1.274$, $p = .002$; Figure 4d). To further clarify this point, we calculated the partial correlation coefficients between positive symptoms and structural factor scores controlling for global band task-related modulation ($r = -.459$, $p = .006$) and between positive symptoms and global band task-related modulation controlling for structural network values ($r = .432$, $p = .01$), supporting the independence of the associations.

## 3.4 | Confounding factors

Duration of illness was inversely associated to structural factor scores ($r = -.599$, $p = .001$). Thus, larger duration would imply smaller dMRI-CLC and dMRI-D as well as longer dMRI-PL. Current antipsychotic dose was not significantly related to structural ($-.069 < r < .148$, $p = $ n. s.) nor functional ($-.040 < r < .183$, $p = $ n.s.) graph-theory parameters.

## 4 | DISCUSSION

Global band network characteristics a baseline in control and its task-related modulation in patients were predicted by structural network parameters. EEG-PL and EEG-CLC in the global band and EEG-D in the theta band showed a significant task-related modulation only in controls after adjustment for multiple comparisons. Although unadjusted, patients showed larger dMRI-PL, higher prestimulus EEG-D at both global and theta bands and reduced functional task-related modulation of EEG-PL at the theta band, without any significant association between these structural and functional alterations. In patients, structural connectivity and theta task-related modulation respectively predicted positive symptoms and cognition.

Network parameters have been calculated from scalp sensors in this work. Therefore, the connectivity estimates are not derived from true sources of the corresponding activity involved in task processing. Volume conduction effects imply that signals from different sources arrive to different sensors, hampering the estimation of the connectivity among the original activity sources (Brunner, Billinger, Seeber, Mullen, & Makeig, 2016; Van de Steen et al., 2016). Our functional estimates are therefore to be considered just a global outline of the functional network characteristics and their modulation with cognitive activity. However, this outline may contain useful information regarding characteristics such as local clustering, mean PL and density of functional connections. They can be relevant to understand differences between patients and controls in terms of prestimulus network organization and their change with cognition. Source estimates using procedures such as low-resolution tomography might allow identifying activity sources from which PLV values could be calculated and among which structural connectivity could be assessed. This approach would be useful to describe effective connectivity relations among these sources, which can be of interest for the pathophysiology of psychosis. Those procedures, however, are not completely reliable, and the inverse solution problem remains unsolved. Therefore, the functional global outline here describe can hold a significant value, in particular its fast modulation with cognition; although only indirectly reflecting the characteristics of the underlying sources.

We calculated structural connectivity parameters using FA values from white matter tracts linking anatomical regions and functional connectivity using phase similarity of EEG signals between sensors. Both measurements summarized the same properties of the respective networks, and the prediction of global band prestimulus (controls) and task-related modulation (patients) functional values from structural scores supports the relation of both kinds of networks. Caution is necessary when considering these relations, given the above mentioned possible influence of volume conduction effects. Remarkably, abnormalities in structural and functional networks were unrelated in the patients.

The lower factor scores in the patients for structural connectivity (positively loaded for dMRI-CLC and dMRI-D and inversely related to dMRI-PL), suggest a reduced integrity of white matter connectivity in schizophrenia among nearby (reflected in lower CLC) and distant (longer PL) regions. The larger dMRI-PL in our patients is coherent with reports of reduction of global communication paths (Griffa et al., 2015; van den Heuvel et al., 2013) and lower FA in schizophrenia, likely reflecting alterations of long-range tracts (Ellison-Wright & Bullmore, 2009; Patel et al., 2011).

To our notice, no previous study has explored the structural underpinnings of alterations of fast task-related modulation in functional networks in schizophrenia. Odd-ball task performance involves the coordination of different brain regions (Linden et al., 1999). For both groups, EEG-PL and EEG-CLC in the global band increased from prestimulus to response windows, which imply that widespread local task-related activations elongate mean EEG-PL and increase EEG-CLC. In our cases, factor scores summarizing structural network (positively associated to dMRI-CLC and dMRI-D, and negatively to dMRI-PL) inversely predicted EEG-PL and EEG-CLC task-related modulation in the global band in patients. Thus, patients with smaller dMRI-CLC and dMRI-D, and larger dMRI-PL, would show a smaller global band EEG-CLC and EEG-PL modulation. However, as compared with controls, patients did not show a deficit of functional EEG-PL task-related modulation in the global band, raising doubts about the significance for

schizophrenia of that association between structural connectivity and global band modulation.

Instead, we found task-related modulation deficits in patients in the theta band. However, modulation in the global band was not decreased in patients, which may relate to the relatively larger involvement of theta oscillations in P300 performance as shown by relative power and median frequency analysis during this task (Bachiller et al., 2014). Using different methodologies, smaller increases of theta power have been found for schizophrenia patients during P300 tasks (Bachiller et al., 2014; Doege et al., 2009). Taken together, this suggests a higher impact on theta than global band connectivity in schizophrenia. Since theta oscillations have a role in synchronization between distant regions (von Stein, Chiang, & Konig, 2000), the task-related modulation deficit in theta suggests a decreased capacity for integrating activity across cortical regions in schizophrenia, which would be not closely associated to anatomical connectivity deficits according to our results.

Such relative independence of structural and functional connectivity alterations surprised us, but could be explained by data showing that functional connectivity exists between regions without direct anatomical connection (Adachi et al., 2012; Honey et al., 2009). Thus, deficits of functional integration (in the theta band) would not require altered structural substrates. Coordination of activity between distant regions may be established indirectly, since functional connectivity is high among regions with common efferences to third regions, which may convey information to higher regions and may also receive similar afferences (Adachi et al., 2012). Therefore, the alteration in relevant cortical hubs reported in schizophrenia (van den Heuvel et al., 2013) may hamper the synchronization of regions not directly linked via with matter tracts. Although other data using anatomical and functional MRI show a substantial correspondence between the corresponding networks (Hagmann et al., 2008), this relation had not been assessed yet with EEG data. Considering all this, we must underline that structural deficits were found in our patients (larger dMRI-PL and lower factor scores) and were predictive of positive symptoms. This suggests the coexistence of alterations in both structural and functional networks (in the theta band) within schizophrenia, but not necessarily in the same cases. In other words, either both unrelated functional and structural networks alterations are found in schizophrenia or they are characteristics of different schizophrenia subgroups. The latter possibility seems favored by recent reports supporting that structural connectivity values can segregate biologically valid clusters within schizophrenia (Lubeiro et al., 2016; Sun et al., 2015; Wheeler et al., 2015). Using EEG, both no difference (Jhung et al., 2013; Rubinov et al., 2009) and a decrease (Micheloyannis et al., 2006) of CLC at rest were reported in schizophrenia, which may be coherent with that possibility.

Remarkably, prestimulus EEG-D is higher in the patients. The density is the mean network degree (i.e., a measure of the network strength), implying a functional over-connectivity at rest in schizophrenia. This result is in agreement with the increased prefrontal functional connectivity reported in schizophrenia (Anticevic et al., 2015). The different patterns of dMRI-D and EEG-D in patients, and the lack of a significant relation between them, support the independence of the alterations in both networks. Speculatively, the increased EEG-D might

relate to the deficit in GABA function observed in schizophrenia (Gonzalez-Burgos, Fish, & Lewis, 2011; Thakkar et al., 2017), which could lead to hyper-synchronization. In our study, functional connectivity is based on PLV values; thus, larger prestimulus theta EEG-D values suggest and excess of synchronization in the patients in this band, which could have a ceiling effect on task-related synchronization and might hamper theta EEG-D modulation. Therefore, an inhibitory transmission deficit could justify both the increased baseline D values and the lower modulation in the theta band, given its large implication in P300 task performance (Bachiller et al., 2014; Doege et al., 2009). This possible dependence on inhibitory function might also justify the lack of a significant prediction of theta modulation by structural connectivity.

The increase in theta task-related modulation values (i.e., larger functional density, CLC and PL in this band) predicted better cognition in the patients. There was only one cognitive factor, which is not surprising since the assessment instrument (BACS) included the dimensions where performance was previously found decreased in schizophrenia. That predictive relationship suggests that cognitive deficit is secondary to the decreased capacity of modulating the functional network in the theta band, perhaps indicating a lesser capacity to integrate the activity of different areas in a task.

Our study is limited by the sample size of patients with both structural and functional network data available. A larger sample would be needed to test the hypothesis of distinct schizophrenia clusters based on structural connectivity. In addition, the assessment of nodal parameters could be of interest. However, connectivity analysis at the sensor level is very problematic due to effects of field spread (Schoffelen & Gross, 2009). Therefore, future studies should also be focused on increasing the number of EEG electrodes to provide more accurate results. Moreover, we cannot rule out an effect of treatment, although antipsychotic doses were unrelated to structural and functional graph parameters. It must be also noted that all EEG measures are influenced by volume conduction. In order to minimize this effect, a well-known strategy is based on the assumption that volume conduction affects the connectivity estimates in a similar way in two different experimental contrasts, such as prestimulus and response conditions (Bastos & Schoffelen, 2016). With regard to the use of dMRI-based connectivity, the accuracy of the cortical segmentation and the choice of the tractography method influence the obtained connectivity matrices. Although FA is the most usual dMRI descriptor for white matter integrity, it cannot identify the ultimate origin of connectivity alterations.

We may conclude that task-related modulation deficit in the theta band in schizophrenia is independent from deviation from normal structural network properties. This, considered together with the different correlates of functional and structural connectivity alterations, might support different clusters within the schizophrenia syndrome.

ORCID

*Vicente Molina* http://orcid.org/0000-0003-2457-2487

## REFERENCES

Adachi, Y., Osada, T., Sporns, O., Watanabe, T., Matsui, T., Miyamoto, K., & Miyashita, Y. (2012). Functional connectivity between anatomically unconnected areas is shaped by collective network-level effects in the macaque cortex. *Cerebral Cortex*, 22(7), 1586–1592.

Anticevic, A., Hu, X., Xiao, Y., Hu, J., Li, F., Bi, F., ... Gong, Q. (2015). Early-course unmedicated schizophrenia patients exhibit elevated prefrontal connectivity associated with longitudinal change. *Journal of Neuroscience*, 35(1), 267–286.

Bachiller, A., Diez, A., Suazo, V., Dominguez, C., Ayuso, M., Hornero, R., ... Molina, V. (2014). Decreased spectral entropy modulation in patients with schizophrenia during a P300 task. *European Archives of Psychiatry and Clinical Neuroscience*, 264(6), 533–543.

Bachiller, A., Poza, J., Gomez, C., Molina, V., Suazo, V., & Hornero, R. (2015a). A comparative study of event-related coupling patterns during an auditory oddball task in schizophrenia. *Journal of Neural Engineering*, 12, 016007.

Bachiller, A., Romero, S., Molina, V., Alonso, J. F., Mananas, M. A., Poza, J., & Hornero, R. (2015b). Auditory P3a and P3b neural generators in schizophrenia: An adaptive sLORETA P300 localization approach. *Schizophrenia Research*, 169, 318–325.

Bastos, A. M., & Schoffelen, J. M. (2016). A tutorial review of functional connectivity analysis methods and their interpretational pitfalls. *Frontiers in Systems Neuroscience*, 9, 175.

Bledowski, C., Prvulovic, D., Hoechstetter, K., Scherg, M., Wibral, M., Goebel, R., & Linden, D. E. (2004). Localizing P300 generators in visual target and distractor processing: A combined event-related potential and functional magnetic resonance imaging study. *Journal of Neuroscience*, 24(42), 9353–9360.

Bob, P., Palus, M., Susta, M., & Glaslova, K. (2008). EEG phase synchronization in patients with paranoid schizophrenia. *Neurosciecne Letters*, 447(1), 73–77.

Bohlken, M. M., Brouwer, R. M., Mandl, R. C., Van den Heuvel, M. P., Hedman, A. M., De Hert, M., ... Hulshoff Pol, H. E. (2016). Structural Brain Connectivity as a Genetic Marker for Schizophrenia. *JAMA Psychiatry*, 73(1), 11–19.

Bressler, S. L., Coppola, R., & Nakamura, R. (1993). Episodic multiregional cortical coherence at multiple frequencies during visual task performance. *Nature*, 366(6451), 153–156.

Brunner, C., Billinger, M., Seeber, M., Mullen, T. R., & Makeig, S. (2016). Volume conduction influences scalp-based connectivity estimates. *Frontiers in Computational Neuroscience*, 10, 121.

Bullmore, E., & Sporns, O. (2009). Complex brain networks: Graph theoretical analysis of structural and functional systems. *Nature Reviews Neuroscience*, 10(3), 186–198.

Collin, G., Scholtens, L. H., Kahn, R. S., Hillegers, M. H. J., & van den Heuvel, M. P. (2017). Affected anatomical rich club and structural-functional coupling in young offspring of schizophrenia and bipolar disorder patients. *Biological Psychiatry*, 82(10), 746–755.

Dehaene, S., & Changeux, J. P. (2011). Experimental and theoretical approaches to conscious processing. *Neuron*, 70(2), 200–227.

Desikan, R. S., Segonne, F., Fischl, B., Quinn, B. T., Dickerson, B. C., Blacker, D., ... Killiany, R. J. (2006). An automated labeling system for subdividing the human cerebral cortex on MRI scans into gyral based regions of interest. *Neuroimage*, 31(3), 968–980.

Dhollaner, T., & Connelly, A. (2016). Unsupervised 3-tissue response function estimation from single-shell or multi-shell diffusion mr data without a co-registered t1 image. In *ISMRM Workshop on Breaking the Barriers of Diffusion MRI*. (vol. 5).

Di Biase, M. A., Cropley, V. L., Baune, B. T., Olver, J., Amminger, G. P., Phassouliotis, C., ... Zalesky, A. (2017). White matter connectivity disruptions in early and chronic schizophrenia. *Psychological Medicine*, 47(16), 2797–2810.

Doege, K., Bates, A. T., White, T. P., Das, D., Boks, M. P., & Liddle, P. F. (2009). Reduced event-related low frequency EEG activity in schizophrenia during an auditory oddball task. *Psychophysiology*, 46(3), 566–577.

Ellison-Wright, I., & Bullmore, E. (2009). Meta-analysis of diffusion tensor imaging studies in schizophrenia. *Schizophrenia Research*, 108(1–3), 3–10.

Fischl, B., van der, K., A., Destrieux, C., Halgren, E., Segonne, F., Salat, D. H., ... Dale, A. M. (2004). Automatically parcellating the human cerebral cortex. *Cerebral Cortex*, 14, 11–22.

Gomez-Pilar, J., Lubeiro, A., Poza, J., Hornero, R., Ayuso, M., Valcarcel, C., ... Molina, V. (2017). Functional EEG network analysis in schizophrenia: Evidence of larger segregation and deficit of modulation. *Progress in Neuropsychopharmacology and Biological Psychiatry*, 76, 116–123.

Gomez-Pilar, J., Poza, J., Bachiller, A., Gomez, C., Nuñez, P., Lubeiro, A., ... Hornero, R. (2018). Quantification of graph complexity based on the edge weight distribution balance: Application to brain networks. *International Journal of Neural Systems*, 28(01), 1750032.

Gonzalez-Burgos, G., Fish, K. N., & Lewis, D. A. (2011). GABA neuron alterations, cortical circuit dysfunction and cognitive deficits in schizophrenia. *Neural Plastics*, 2011, 1.

Griffa, A., Baumann, P. S., Ferrari, C., Do, K. Q., Conus, P., Thiran, J. P., & Hagmann, P. (2015). Characterizing the connectome in schizophrenia with diffusion spectrum imaging. *Human Brain Mapping*, 36(1), 354–366.

Hagmann, P., Cammoun, L., Gigandet, X., Meuli, R., Honey, C. J., Wedeen, V. J., & Sporns, O. (2008). Mapping the structural core of human cerebral cortex. *PLoS Biology*, 6(7), e159.

Honey, C. J., Sporns, O., Cammoun, L., Gigandet, X., Thiran, J. P., Meuli, R., & Hagmann, P. (2009). Predicting human resting-state functional connectivity from structural connectivity. *Proceedings of the National Academy of Sciences of the United States of /America*, 106(6), 2035–2040.

Honey, C. J., Thivierge, J. P., & Sporns, O. (2010). Can structure predict function in the human brain?. *Neuroimage*, 52(3), 766–776.

Jhung, K., Cho, S. H., Jang, J. H., Park, J. Y., Shin, D., Kim, K. R., ... An, S. K. (2013). Small-world networks in individuals at ultra-high risk for psychosis and first-episode schizophrenia during a working memory task. *Neuroscience Letters*, 535, 35–39.

Jones, J. T., DiFrancesco, M., Zaal, A. I., Klein-Gitelman, M. S., Gitelman, D., Ying, J., & Brunner, H. I. (2015). Childhood-onset lupus with clinical neurocognitive dysfunction shows lower streamline density and pairwise connectivity on diffusion tensor imaging. *Lupus*, 24(10), 1081–1086.

Kambeitz, J., Kambeitz-Ilankovic, L., Cabral, C., Dwyer, D. B., Calhoun, V. D., van den Heuvel, M. P., ... Malchow, B. (2016). Aberrant functional whole-brain network architecture in patients with schizophrenia: A meta-analysis. *Schizophrenia Bulletin*, 42(Suppl 1), S13–S21.

Kay, S. R., Fiszbein, A., & Opler, L. A. (1987). The positive and negative syndrome scale (PANSS) for schizophrenia. *Schizophrenia Bulletin*, 13(2), 261–276.

Lachaux, J. P., Rodriguez, E., Martinerie, J., & Varela, F. J. (1999). Measuring phase synchrony in brain signals. *Human Brain Mapping*, 8(4), 194–208.

Linden, D. E., Prvulovic, D., Formisano, E., Vollinger, M., Zanella, F. E., Goebel, R., & Dierks, T. (1999). The functional neuroanatomy of

target detection: An fMRI study of visual and auditory oddball tasks. *Cerebral Cortex*, 9(8), 815–823.

Lo, C. Y., Su, T. W., Huang, C. C., Hung, C. C., Chen, W. L., Lan, T. H., . . . Bullmore, E. T. (2015). Randomization and resilience of brain functional networks as systems-level endophenotypes of schizophrenia. *Proceedings of the National Academy of Sciences of the United States of America*, 112(29), 9123–9128.

Lubeiro, A., Rueda, C., Hernandez, J. A., Sanz, J., Sarramea, F., & Molina, V. (2016). Identification of two clusters within schizophrenia with different structural, functional and clinical characteristics. *Progress in Neuropsychopharmacology & Biological Psychiatry*, 64, 79–86.

Ma, S., Calhoun, V. D., Eichele, T., Du, W., & Adalı, T. (2012). Modulations of functional connectivity in the healthy and schizophrenia groups during task and rest. *Neuroimage*, 62(3), 1694–1704.

Martin-Santiago, O., Gomez-Pilar, J., Lubeiro, A., Ayuso, M., Poza, J., Hornero, R., . . . Molina, V. (2016). Modulation of brain network parameters associated with subclinical psychotic symptoms. *Progress Neuropsychopharmacology & Biological Psychiatry*, 66, 54–62.

Micheloyannis, S., Pachou, E., Stam, C. J., Breakspear, M., Bitsios, P., Vourkas, M., . . . Zervakis, M. (2006). Small-world networks and disturbed functional connectivity in schizophrenia. *Schizophrenia Research*, 87(1–3), 60–66.

Molina, V., Lubeiro, A., Soto, O., Rodriguez, M., Álvarez, A., Hernández, R., & de Luis-García, R. (2017). Alterations in prefrontal connectivity in schizophrenia assessed using diffusion magnetic resonance imaging. *Progress in Neuropsychopharmacology & Biology Psychiatry*, 76, 107–115.

Nunez, P., Poza, J., Bachiller, A., Gomez-Pilar, J., Lubeiro, A., Molina, V., & Hornero, R. (2017). Exploring non-stationarity patterns in schizophrenia: Neural reorganization abnormalities in the alpha band. *Journal of Neural Engineering*, 14(4), 046001.

Patel, S., Mahon, K., Wellington, R., Zhang, J., Chaplin, W., & Szeszko, P. R. (2011). A meta-analysis of diffusion tensor imaging studies of the corpus callosum in schizophrenia. *Schizophrenia Research*, 129(2–3), 149–155.

Patenaude, B., Smith, S. M., Kennedy, D. N., & Jenkinson, M. (2011). A Bayesian model of shape and appearance for subcortical brain segmentation. *Neuroimage*, 56(3), 907–922.

Rubinov, M., Knock, S. A., Stam, C. J., Micheloyannis, S., Harris, A. W., Williams, L. M., & Breakspear, M. (2009). Small-world properties of nonlinear brain activity in schizophrenia. *Human Brain Mapping*, 30(2), 403–416.

Rubinov, M., & Sporns, O. (2010). Complex network measures of brain connectivity: Uses and interpretations. *Neuroimage*, 52(3), 1059–1069.

Salvador, R., Pena, A., Menon, D. K., Carpenter, T. A., Pickard, J. D., & Bullmore, E. T. (2005). Formal characterization and extension of the linearized diffusion tensor model. *Human Brain Mapping*, 24(2), 144–155.

Schoffelen, J. M., & Gross, J. (2009). Source connectivity analysis with MEG and EEG. *Human Brain Mapping*, 30(6), 1857–1865.

Segarra, N., Bernardo, M., Gutierrez, F., Justicia, A., Fernandez-Egea, E., Allas, M., . . . Keefe, R. S. (2011). Spanish validation of the Brief Assessment in Cognition in Schizophrenia (BACS) in patients with schizophrenia and healthy controls. *European Psychiatry*, 26(2), 69–73.

Shim, M., Kim, D. W., Lee, S. H., & Im, C. H. (2014). Disruptions in small-world cortical functional connectivity network during an auditory oddball paradigm task in patients with schizophrenia. *Schizophrenia Research*, 156(2–3), 197–203.

Smith, S. M. (2002). Fast robust automated brain extraction. *Human Brain Mapping*, 17(3), 143–155.

Spencer, K. M., Nestor, P. G., Niznikiewicz, M. A., Salisbury, D. F., Shenton, M. E., & McCarley, R. W. (2003). Abnormal neural synchrony in schizophrenia. *Journal of Neuroscience*, 23, 7407–7411.

Stam, C. J., de Haan, W., Daffertshofer, A., Jones, B. F., Manshanden, I., van Cappellen van Walsum, A. M., . . . Scheltens, P. (2009). Graph theoretical analysis of magnetoencephalographic functional connectivity in Alzheimer's disease. *Brain*, 132(1), 213–224.

Sui, J., Yu, Q., He, H., Pearlson, G. D., & Calhoun, V. D. (2012). A selective review of multimodal fusion methods in schizophrenia. *Frontiers in Human Neuroscience*, 6, 27.

Sun, H., Lui, S., Yao, L., Deng, W., Xiao, Y., Zhang, W., . . . Gong, Q. (2015). Two patterns of white matter abnormalities in medication-naive patients with first-episode schizophrenia revealed by diffusion tensor imaging and cluster analysis. *JAMA Psychiatry*, 72(7), 678–686.

Thakkar, K. N., Rosler, L., Wijnen, J. P., Boer, V. O., Klomp, D. W., Cahn, W., . . . Neggers, S. F. (2017). 7T Proton magnetic resonance spectroscopy of gamma-aminobutyric acid, glutamate, and glutamine reveals altered concentrations in patients with schizophrenia and healthy siblings. *Biological Psychiatry*, 81(6), 525–535.

Tournier, J. D., Calamante, F., & Connelly, A. (2007). Robust determination of the fibre orientation distribution in diffusion MRI: Non-negativity constrained super-resolved spherical deconvolution. *Neuroimage*, 35(4), 1459–1472.

Van de Steen, F., Faes, L., Karahan, E., Songsiri, J., Valdes-Sosa, P. A., & Marinazzo, D. (2016). Critical comments on EEG sensor space dynamical connectivity analysis. *Brain Topography*, [Epub ahead of print].

van den Heuvel, M. P., Mandl, R. C., Stam, C. J., Kahn, R. S., & Hulshoff Pol, H. E. (2010). Aberrant frontal and temporal complex network structure in schizophrenia: A graph theoretical analysis. *The Journal of Neuroscience: The Official Journal of the Society for Neuroscience*, 30 (47), 15915–15926.

van den Heuvel, M. P., Sporns, O., Collin, G., Scheewe, T., Mandl, R. C., Cahn, W., . . . Kahn, R. S. (2013). Abnormal rich club organization and functional brain dynamics in schizophrenia. *JAMA Psychiatry*, 70(8), 783–792.

van Diessen, E., Numan, T., van Dellen, E., van der Kooi, A. W., Boersma, M., Hofman, D., . . . Stam, C. J. (2015). Opportunities and methodological challenges in EEG and MEG resting state functional brain network research. *Clinical Neurophysiology*, 126(8), 1468–1481.

Varela, F., Lachaux, J. P., Rodriguez, E., & Martinerie, J. (2001). The brainweb: Phase synchronization and large-scale integration. *Nature Reviews Neuroscience*, 2(4), 229–239.

von Stein, A., Chiang, C., & Konig, P. (2000). Top-down processing mediated by interareal synchronization. *Proceedings of the National Academy of Sciences of the United States of America*, 97(26), 14748–14753.

Wheeler, A. L., Wessa, M., Szeszko, P. R., Foussias, G., Chakravarty, M. M., Lerch, J. P., . . . Voineskos, A. N. (2015). Further neuroimaging evidence for the deficit subtype of schizophrenia. A cortical connectomics analysis. *JAMA Psychiatry*, 72(5), 446–455.

Yu, Q., Sui, J., Rachakonda, S., He, H., Gruner, W., Pearlson, G., . . . Calhoun, V. D. (2011). Altered topological properties of functional network connectivity in schizophrenia during resting state: A small-world brain network study. *PLoS One*, 6(9), e25423.

Zhang, Y., Brady, M., & Smith, S. (2001). Segmentation of brain MR images through a hidden Markov random field model and the expectation-maximization algorithm. *IEEE Transactions on Medical Imaging*, *20*(1), 45–57.

## SUPPORTING INFORMATION

Additional Supporting Information may be found online in the supporting information tab for this article.